*Final Draft*
**of the original manuscript:**

Onken, R.; Alvarez, A.; Fernandez, V.; Vizoso, G.; Basterretxea, G.; Tintore, J.; Haley, P.; Nacini, E.:

**A forecast experiment in the Balearic Sea**

In: Journal of Marine Systems (2007) Elsevier

DOI: 10.1016/j.jmarsys.2007.05.008

# A forecast experiment in the Balearic Sea

by

**Reiner Onken**
Institute for Coastal Research
GKSS Research Centre
Max-Planck-Straße 1, 21052 Geesthacht, Germany
onken@gkss.de
phone: +49-4152-87-1546, fax: +49-4152-87-1525

**Alberto Álvarez, Vicente Fernández, Guillermo Vizoso, Gotzon Basterretxea, Joaquín Tintoré**
IMEDEA
C/ Miquel Marquès 21, 07190 Esporles, Mallorca, Spain

**Patrick Haley, jun.**
Harvard University
29 Oxford Street, Cambridge, MA 02138-2901, USA

and

**Elvio Nacini**
NATO Undersea Research Centre
Viale San Bartolomeo 400
19138 La Spezia, Italy

submitted to the *Journal of Marine Systems*

January 15, 2007

# Abstract

A forecast experiment in the Balearic Sea is presented which is based on the Harvard Ocean Prediction System (HOPS). HOPS is modular, containing a high-resolution primitive equations model, packages for Objective Analysis and data assimilation (Optimum Interpolation), an interface to implement atmospheric forcing and another interface for one-way nesting of HOPS into any other larger scale circulation model. Here, to prevent false advection from open boundaries, HOPS is nested into the basin scale DieCAST model (Dietrich et al. 2004) and atmospheric forcing fields were provided in terms of HIRLAM fields by the Spanish National Institute of Meteorology.

The forecast capability of HOPS is demonstrated in terms of a hindcast experiment, utilising two observational data sets of a subregion of the Balearic Sea which were acquired in mid September and early October 2002. While the data of the first survey is used for model initialisation, that of the second survey serves for validation of the forecast products. The forecast skill of the system is evaluated quantitatively by three different objective methods, comparing the *rms* difference of vertical profiles and horizontal fields, and pattern correlations, both for temperature and salinity. In five out of six cases, the forecasted fields are closer to the validation data set than the fields used for initialisation, i.e. the forecast beats persistence and the forecast is successful.

Taking into account further available options of HOPS (implementation of additional tracers, tracking of Lagrangian particles, biological modules, two-way nesting), the system is operational for a wide field of possible applications.



Keywords: Mediterranean Sea, Balearic Sea, operational model, forecast model, HOPS, SOFT

# 1 Introduction

There is an increased demand to assess the present and predict the future state of the oceanic environment, a task which can only be accomplished by the use of numerical ocean nowcast and forecast systems. These systems in general consist of observational networks, data assimilation schemes and dynamical forecast models (Robinson et al. 1996). In the present paper, such a system is presented, enabling operational forecasts for the Balearic Sea (Western Mediterranean) on time scales of the order of days to weeks. The operationality, together with a forecast skill evaluation, is demonstrated in terms of a hindcast experiment. Ocean forecasts on such time scales are relevant for numerous customers: fishermen are interested in predictions of the mesoscale variability of temperature and salinity, because they know about the favourite location of fish, e.g. in the vicinity of ocean fronts (Malakoff 2004). For tourism managers it is important to know about the advection of harmful algae blooms (Hoagland et al. 2002). In case of fighting an oil-spill, it is vital to have reliable forecasts of the spreading of the oil patch (Daniel et al. 2005), and military institutions are primarily interested in changes of the underwater sound velocity structure (Harding et al. 2005).

Presently, in the framework of the European project MFSTEP (**M**editerranean **F**orecasting **S**ystem **T**oward **E**nvironmental **P**redictions), there are numerous operational forecast models under development for the Mediterranean Sea, ranging from basin-scale (horizontal resolution 1/16°) over regional (3.5 km) to shelf scale (1.5 km, see Pinardi et al. 2003, and http://www.bo.ingv.it/mfstep/). In particular, there is a regional model of the Western Mediterranean under construction, encompassing the Ligurian Sea, the Gulf of Lions, and the northern part of the Balearic Sea. As the southern boundary of that model is at about the Ibiza latitude (Fig. 1), it is not suitable for predictions of the Balearic Sea

dynamics because the Ibiza Channel and the Mallorca Channel are not properly resolved. However, as shown by Pinot et al. (1998), the flow through these channels is of first order importance for the interior dynamics of the Balearic Sea.

The present investigation is intended to fill that gap: the prognostic Harvard Ocean Prediction System (HOPS) model has been set up for the Balearic Sea at high horizontal and vertical resolution. To prevent contamination of the dynamics in the interior of the model domain from the open boundaries, the HOPS domain is one-way nested into another basin-scale model of the Mediterranean Sea.

The operationality of the system is enabled by several factors: (i) in the vertical, HOPS uses terrain-following coordinates; hence, complex topography in the model is close to reality. (ii) The 2-km horizontal resolution selected for HOPS makes use of the resolution of the best available topography, which is at one geographical minute. (iii) In the vertical direction, the model domain is divided in 30 layers, chosen to fully resolve the mixed-layer and the thermocline. (iv) Intermittent assimilation of observational data keeps the model on track. (v) Momentum, heat and water fluxes are provided by an operational weather prediction model, and (vi), HOPS can be run on a portable personal computer, the turnaround being less than a day for a one-week forecast range.

The feasibility and product quality of HOPS is demonstrated in terms of a hindcast experiment taking place in September/October 2002. For that period of time, two quasi-synoptic observational data sets were available for the same area. The time-lag between these snapshots is about three weeks, making them suitable for model initialisation and validating the forecast.

This article is structured as follows: the next section is related to the geographic and oceanographic setting, in Section 3 the observational data sets used for model initialisation and validation are presented, and HOPS is described in Section 4. The forecast results

together with a forecast skill evaluation are displayed in Section 5, followed by a discussion in Section 6 and Summary and Conclusions in Section 7.

# 2 Geographic and oceanographic context

The Balearic Sea is a semi-enclosed basin bounded by the Iberian peninsula in the west and northwest, and in the southeast by the archipelago of the Balearic islands (Fig.1). In the northeast it is open to the Gulf of Lions, while in the southeast it is connected to the Algerian Basin by means of three gaps in the islands chain: the Ibiza, Mallorca and Minorca Channels. While the sill depths of the western and the central channel are 650 m and 725 m, respectively, that of the Minorca Channel is shallower than 200 m, hence the deep channels are potential pathways for the exchange of Levantine Intermediate Water (LIW), while the easternmost channel is not. The maximum depth of the basin is around 2800 m, roughly 100 km north of Mallorca. The mean shelf slopes are of the order of a few percent, which is rather gentle for Mediterranean conditions; only around Minorca the slopes are steeper, in places exceeding 10%.

The 0–150 m surface layer of the Balearic Sea is dominated by water masses of Atlantic origin: recent Modified Atlantic Water (MAW) originating from the Strait of Gibraltar invades the basin from the south through the Ibiza Channel, and older MAW comes from the north along the Iberian shelf slope by means of the Liguro-Provençal-Catalan Current (Pinot et al. 1995). The latter continues south along the slope and partly keeps on heading farther south leaving the Balearic Sea through the Ibiza and Mallorca Channels. The other part makes a cyclonic turn at about the latitude of the Mallorca Channel and joins there the MAW flow from the south forming the Balearic Current which is closely attached to the northeastern slopes of Mallorca and Minorca, and leaves the basin heading northeast.

The major components of this basin-scale circulation pattern, i.e. the Liguro-Provençal-Catalan Current and the Balearic Current, are accompanied by fronts – the Catalan Front and the Balearic Front. These fronts are frequently subject to instability processes (Pinot et al. 1994), permitting a cross-frontal turbulent exchange of properties. Below the MAW and reaching down to approximately 700-m depth, LIW is the characteristic water mass. The LIW is coming from the north as well and joins the large-scale cyclonic circulation similar to the MAW (Álvarez et al. 1994). Finally, the deep basin is filled by Western Mediterranean Deep Water originating from deep convection events in the Gulf of Lions (Millot 1987).

A special feature of the Gulf of Lions and the Balearic Basin are numerous submarine canyons cutting into the continental slope. The most prominent ones are the Blanes Canyon and the Palamós Canyon, the impact of which on the near-coastal flow has been recently explored by Álvarez et al. (1996) and Ardhuin et al. (1999). The latter using a numerical model, were able to demonstrate that such canyons, oriented perpendicular to a coastal jet, support anticyclonic motion.

# 3 The observational programme

The observational data sets utilised for initialisation of the forecast system and validation of the forecast results were acquired during two campaigns conducted in the framework of the European Union project SOFT (**S**atellite Based **O**cean **F**orecast Sys**T**em). The first survey (SOFT-I), which took place September 15–20, 2002, consisted of 56 CTD (Conductivity-Temperature-Depth) casts reaching down to about 500-m depth and was located northwest of Mallorca between the Balearic Islands and the Spanish mainland (Figs. 1, 2). The second survey (SOFT-II) was intended as a repeat survey, taking place

about three weeks later October 6–9. The casts were taken at exactly the same positions as those of SOFT-I. However, due to bad weather conditions, the SOFT-II campaign was aborted earlier than originally planned and only 38 CTD stations were occupied. In addition to the CTD casts, high-quality velocity data of the upper ≈250-m flow field are available from a ship-mounted ADCP. Infrared images of sea surface temperature were taken from the NOAA 12 and NOAA 17 satellites, and made available by the NATO Undersea Research Centre in La Spezia (Italy).

# 4 Setup of forecast model runs

HOPS is utilised for the forecasts described below. HOPS is a collection of program packages containing everything which is needed for ocean forecasting. The heart of HOPS is a primitive equations (PE) model, surrounded by various modules necessary for setting up the model domain and the grid, conditioning of bathymetry, nesting, management of observational data, preparation of assimilation fields, etc. (Robinson 1996, 1999, Robinson et al. 1996, Lozano et al. 1996). In the following, only those modules of HOPS are described which are used for the model runs presented below.

## 4.1 The primitive equations model

The dynamical model used in this study solves the primitive equations, assuming that the fluid is hydrostatic and the Boussinesq approximation is valid (Spall and Robinson 1990, Lermusiaux 1997). The vertical boundary conditions are that of no normal flow at the surface (rigid-lid) and at the bottom. Terrain-following coordinates are used in the vertical, which enable the model surfaces to smoothly follow the bathymetry.

Horizontal subgrid scale processes are parameterised by a 4-3-1 (fourth order, three

times, every time step) Shapiro filter (Shapiro 1970, Robinson and Walstad 1987) for momentum, and a 4-1-1 filter for tracers, vorticity and transport. Vertical diffusion is formulated in terms of a Richardson-number dependent scheme similar to that of Pacanowski and Philander (1981), using a maximum value of 50 $cm^2\ s^{-1}$ for eddy viscosity when the Richardson number is zero or when the water column is gravitationally unstable. Near the surface, in a "mixing layer", the vertical diffusion is restricted to always being at least 50 $cm^2\ s^{-1}$ . The depth of this mixing layer is proportional to the wind stress. The chosen constant of proportionality, 0.174, means that a wind of 15 knots produces a mixing layer of ≈19m. Near horizontal and vertical rigid boundaries, Rayleigh friction is applied using a Gaussian weighting of distance from the bottom or the coast, respectively (Lermusiaux 1997).

## 4.2 Model domain, bathymetry and grid setup

The model domain extends zonally from about 30′ W to 6°E, and in meridional direction from about 38°N to 43°36′ N (Fig. 1). The bottom is defined by the DBDBV bathymetric data set at 1′ resolution, obtainable from the Naval Oceanographic Office, Stennis Space Center, Mississippi, http://www.navo.navy.mil/. The horizontal grid size is 2 km yielding 207 grid points in west–east and 314 points in south–north direction. Vertically, the domain is divided in 30 levels defined in terms of terrain-following $\sigma$-coordinates (Spall and Robinson 1989, Haley 2001). The use of such coordinates requires careful handling of the bathymetry data. First of all, the data is interpolated on the horizontal model grid and all elevations above -10 m are clipped. This is because the minimum depth to be resolved by the model was set to this value, in part to prevent crowding of $\sigma$-levels. Then, land points are re-introduced by superposition of a high-quality coastline data set. Small-scale roughness is removed by repeated median filtering, before the vertical levels

are defined. Here, special care must be taken that the hydrostatic consistency condition is guaranteed in order to reduce the truncation error of the pressure gradient calculation to tolerable levels (Haney 1991, Lozano et al. 1994, Sloan 1996). As this condition is proportional to $\sigma$, the gradient of the bathymetry and the horizontal grid size, it can be satisfied by optimised positioning of the $\sigma$-levels and by reduction of the bathymetry slope. In the present case, the bottom slope was reduced to a maximum value of 8%, which retains most of the bathymetric details except for the extremely steep slopes along the north coast of Minorca and the southeast coast of Mallorca.

## 4.3 Initial and lateral boundary conditions, atmospheric forcing

A delicate problem of operational ocean models is to find an initial state from which to begin the integration. Attempts have been undertaken to utilise the MODB (obtainable from the University of Liège, http://modb.oce.ulg.ac.be) and GDEM (US Naval Oceanographic Office, Stennis Space Centre, Mississippi, https://www.navo.navy. mil) seasonal and monthly climatologies, but it became immediately evident that the structures provided by those data sets were quite different from the situation diagnosed in September 2002. In detail, the climatological temperature and salinity fields did not at all match the observations of the SOFT-I survey, and transport patterns did not agree with the previously known schemes (Pinot et al. 1994). Therefore, temperature and salinity fields were taken from another large scale primitive equations model of the Mediterranean, the DieCAST model (Dietrich et al. 2004, Fernández et al. 2005).

DieCAST is a primitive equations model, the most important properties of which are fourth-order approximations of the advection and pressure gradient terms. The horizontal resolution varies between 12 km in the south and 10 km in the north. DieCAST was initialised from MED4 climatology (Brasseur et al. 1996) and integrated for 15 years,

reaching an equilibrium after about twelve years. The model is driven by atmospheric forcing in terms of re-analysis fields provided by the European Centre for Medium-Range Weather Forecasts (Reading, United Kingdom).

To utilise the DieCAST output for HOPS initialisation, the three-dimensional temperature and salinity fields of September 10 were extracted and interpolated on the HOPS horizontal and vertical grid. As the DieCAST temperature and salinity fields were also different from the SOFT-I observations, mean temperature and salinity values were calculated on horizontal levels for the SOFT-I area, both from DieCAST and the SOFT-I survey, and the entire DieCAST fields were then shifted towards SOFT-I by the difference of the means level by level. As can be seen from Fig. 3, the SOFT-I temperature in the upper about 80-m depth range is up to 6 K higher than DieCAST, while between 100-m and 500-m depth the DieCAST temperature is about 1 K higher than SOFT-I. Concerning salinity, SOFT-I is fresher than DieCAST close to the surface, and always saltier than DieCAST below.

The generic version of the HOPS PE model applies open boundaries not bounded by coastlines. Although sophisticated algorithms are available to cure this problem (e.g. Orlanski 1976, Spall and Robinson 1990), there is always a tendency for the occurrence of numerical instability or false advection along the open boundaries, especially during long-term integrations. To avoid that, the boundary values of the HOPS domain were replaced by the corresponding DieCAST values: temperature, salinity, total horizontal velocity and the transport streamfunction were extracted from DieCAST in two-days-intervals and then linearly interpolated in time on the HOPS domain boundaries at every time step.

Atmospheric forcing of momentum and surface fluxes of heat and water were provided by the Spanish National Institute of Meteorology in terms of six-hourly fields of the

High Resolution Limited Area Model (HIRLAM, cf. http://hirlam.knmi.nl). While the horizontal resolution of the heat and water fluxes is 0.5°, 10-m winds are resolved higher at 0.2°.

## 4.4 Intermittent assimilation of hydrographic data

Although the HOPS PE model is initialised and the open boundaries are stabilised by the DieCAST solution, it cannot be expected that the structures developed by the PE model are representing any real situation, because DieCAST itself is based on climatology. Therefore, observed data of the CTD casts taken during the SOFT-I survey are assimilated repeatedly into the PE model. Although more sophisticated algorithms have been developed and applied in the recent past (cf. Ferron and Marotzke, 2003), Optimum Interpolation (Robinson et al. 1998) is the assimilation method used here because of the efficiency of computational costs. For that purpose, objective analysis (OA) fields of temperature and salinity have been prepared for the entire SOFT-I period in 24-hour-intervals and centred in time at noon of every day, applying a spatial correlation scale of 20 km and a temporal correlation scale of three days. The selected spatial scale is a compromise between the internal Rossby radius ($\approx$ 15 km in summer) and the distances between CTD stations (10 nautical miles) and between the legs of the survey ($\approx$ 11.5 nautical miles), while the temporal scale is of the order of the Lagrangian time scale in the upper ocean. In total, seven fields are available September 15–21 (Fig. 4). First, OA is carried out on 29 horizontal levels between the sea surface and the maximum extent of the casts at 500 m. The resultant three-dimensional fields are interpolated vertically on the model $\sigma$-levels using cubic splines.

To relax the PE model towards the temperature and salinity structures observed during SOFT-I, the fields of September 15 are assimilated into the model for the first time on

September 11 (noon), using a rather weak assimilation weight of 0.1. This procedure is repeated three times at noon times of September 12–14, "teaching" the SOFT-I structures to the PE model. Next, from September 14, 18:00h to the nominal time of the OA field on September 15, 12:00h, the same data set is assimilated in six-hour intervals, but now the assimilation weight is steadily increasing from 0.1 at 18:00h, 0.2 at midnight, 0.5 at 06:00h and 0.9 at noon next day. By this method, the assimilation fields are "ramped up" towards the nominal time, forcing the PE model with increasing pressure to the observations. Until noon of September 21, this procedure is repeated day by day every six hours utilising the remaining assimilation cycles of September 16–21. In the same way as the PE model has "learnt" from the observations, a linear "ramping down" procedure is applied when the SOFT-I survey was finished, to prevent that the model "forgets" the reality too quickly. In that sense, the assimilation cycle of September 21 is assimilated repeatedly after its nominal time in six-hour intervals by decreasing the assimilation weight by 0.05 every step. The last assimilation takes place on September 30 at 00:00h, having a rather small weight of just 0.05. By this method, enough freedom is left for the model to develop its own dynamics.

# 5 Forecast results

Results of a forecast run are presented, which is integrated for 30 days from September 10 through October 10, 2002, including both the period of the SOFT-I and SOFT-II surveys. The model is initialised as described above from DieCAST, and open boundary conditions are updated at every time step. As this run is intended to simulate typical operational forecasting conditions, the time varying atmospheric forcing is turned off after September 23, 09:00h, utilising further on only mean fluxes of momentum, heat and water

averaged over the preceeding integration period. This is representing the real situation of September 20 when the last CTD casts were taken, and a reliable weather forecast was available for another 72 hours. By contrast, data assimilation takes place through September 30, and afterwards the model is no more driven by data through October 10.

Four different procedures are applied to assess the performance of the model: first, simulated fields of temperature, salinity and velocity are interpreted in terms of previously known patterns of the Balearic Sea. Then, focusing on the SOFT area, sea surface temperature structures are compared with infrared satellite images, and then modelled structures are compared with real structures obtained from the SOFT-II data set. Finally, the forecast skill of the model is evaluated objectively utilising different methods.

## 5.1 Comparison of patterns with previous knowledge

In Fig. 5, surface temperature, velocity and salinity are displayed at three different instants. The initialisation fields of September 10 as they were taken from DieCAST, are shown in the top panel. It can clearly be seen that the Balearic Sea is the meeting point of two regimes: from the Gulf of Lions, cold and saline water is advected to the south along the Spanish coast by means of the Liguro-Provençal-Catalan Current, opposed by warmer and fresher Atlantic Water entering through the Ibiza and Mallorca Channels. Within the Balearic Sea, these current systems are merging, forming a cyclonic circulation and the Balearic Current. This large scale pattern is in agreement with the earlier findings by Pinot et al. (1994, 1995) and García-Ladona et al. (1996).

During the SOFT-I phase September 15–25 (centre panel), the large scale flow pattern is still present, but the cyclonic loop is distorted by a strong anticyclone sitting right off the Spanish coast at about 41°N. Typical for anticyclones, the near surface density is lower than in the ambient water, expressed by higher temperature and lower salinity. This

may explain the above mentioned temperature and salinity differences between SOFT-I and DieCAST. The eddy, exhibiting a maximum surface flow speed of up to 65 cm $s^{-1}$ is blocking the southward coastal current and forces the inflow from the north to veer eastward at about the same latitude. A fraction of the deviated current is heading right to the east, while the rest is circumventing the eddy and then joining the former cyclonic circulation. At the same time, the southward coastal current south of the anticyclone becomes more intense and narrower, and the Balearic Current is amplifying, exhibiting maximum velocities of close to 50 cm $s^{-1}$ . As there are no observations available in this region, one is left to compare these patterns with other models: the DieCAST model of Fernández et al. (2005, their Fig. 4) shows the same patterns and the velocity magnitude is in agreement as well. The same is also visible in the operational MFSTEP model (http://www.bo.ingv.it/mfstep) throughout the year. Another feature worth to mention is the anticyclone in the Mallorca Channel, resembling the anticyclonic transport pattern found by García-Ladona et al. (1996). By contrast, no such inflow/outflow pattern is reproduced by the model in the Ibiza Channel.

During the SOFT-II phase September 30 - October 10, (bottom panel), the mean fields have slightly changed. The inflow from the Gulf of Lions is looking now more jet like. The previously mentioned anticyclone has moved to the southwest along the Catalan coast by about 50 km and becoming more intense, the mean speeds being now about 10 cm $s^{-1}$ higher then three weeks earlier. At the former position of this eddy, another anticyclonic flow pattern has started to develop. As this place coincides with the location of the Blanes Canyon, this is supporting the findings by Ardhuin et al. (1999), that the canyons are triggering anticyclonic motion. Another noteworthy feature is the elongated cyclone right over the continental shelf at about the Ibiza latitude, the signal of which is clearly visible in the surface salinity field as well.

## 5.2 Comparison of sea surface temperature with satellite images

Satellite images of sea surface temperature provide another useful tool to validate the structures and evolution of near-surface patterns. Figs. 6 and 7 show the evolution of sea surface temperature in the Northern Balearic Sea as predicted by the model and observed by satellite. The selected region is centred in the SOFT area but displays also the surrounding patterns. The somewhat odd selection of the instants shown is due to the fact that only a handful of cloud free satellite images were available.

The instants displayed in Fig. 6 are related to the situation before any strong data assimilation took place, and it cannot be expected that the predicted and observed fields are matching. Instead, the satellite images were chosen because they impressively show the birth of the anticyclone off the Catalan coast. On September 10, there is apparently an outbreak of cold water directed from northeast to southwest and invading the northern Balearic Sea. The head of the outbreak (this is the Catalan/Balearic Front) is marked by a pair of mushroom-like temperature patterns to the left and the right. Three days later on September 13, the spiral-shaped temperature structure suggests the generation of anticyclonic flow off the coast, and another two days ahead on September 15, the temperature distribution exhibits the well-known pattern of an anticyclonic eddy. By contrast, the simulated temperature fields (left panel) do not indicate any evidence for anticyclonic motion in the respective area. Apparently, the model dynamics is still controlled by the initial conditions and does not yet feel significantly the assimilated SOFT-I in-situ data.

However, on September 26 after finalisation of the SOFT-I campaign (Fig. 7), the eddy is present both in the simulation and in the satellite image. Note that also the position of the eddy centre is modelled correctly and there is also some agreement concerning the cold filament surrounding the eddy and the little meanders southeast of it.

A major issue of comparing the simulated and observed sea surface pattern in Figs. 6 and 7 was to investigate whether the eddy in the model is migrating at the right speed. From the sequence of satellite images it appears that the eddy centre is moving southeast along the shelf break. A rough estimate of the displacement from September 13 to October 5 yields 30 nautical miles or an equivalent phase speed of 2.5 cm $s^{-1}$ . About the same phase speed may be deducted from the simulation for the period September 22 to October 10. Hence, this indicates that in the SOFT area the model dynamics is similar to reality.

## 5.3 Comparison with patterns obtained during SOFT-II

### 5.3.1 Temperature and salinity

Fig. 8 enables a qualitative check of how well the forecasted temperature and salinity fields agree with the observations of the SOFT-II survey. While the observed fields were directly taken from the CTD casts, the corresponding modelled fields are mean values of the forecasts of October 6–9. As the predicted and observed fields below 100-m depth are almost identical, only the upper 100-m depth range is shown. For temperature, the maximum values are close to 24°C for both the model output and the observations. This is indicative for the air-sea heat flux working correctly in the model. The vertical stratification in the model is weaker than in reality, which may be due to unadequate parameterisation of the eddy diffusivity. Concerning the horizontal temperature structure, there is only a zero-order agreement, i.e. there is a common trend of colder water in the north and warmer water in the south. This is probably caused by false advection being discussed below. The same can be said with respect to the vertical stratification and the horizontal structure of salinity. However, the salinity minimum values in all legs do not agree. Apparently, this is due to bad prediction of the position of the Balearic Front (cf.

Fig. 5).

### 5.3.2 Horizontal velocity

In order to assess the quality of the forecast in terms of velocity, the modelled horizontal velocity of October 8 (noon) is compared with ship-board ADCP measurements acquired during SOFT-II. As ADCP observations were only available as vertical layer means, the modelled velocity fields were interpolated on 1-m depth intervals and then vertically averaged between 16 and 25 m, which is the uppermost level of the ADCP observations. Those in turn were mapped on the horizontal model grid by objective analysis. Fig. 9 shows that the velocity scales of the observations and the forecast are rather similar, and there is also some agreement of the structures, namely; the southward flow in the north-east corner of the SOFT-II region, the anticyclonic eddy in the west, and the easterly current at about 4°E, 41°N. By contrast, the predicted strong eastward flow in the south does not match the observations, and also the observed anticlyclonic motion in the centre of the region was not forecasted correctly.

## 5.4 Objective forecast skill evaluation

In the previous subsections it was demonstrated that HOPS is able to predict the evolution of oceanic fields exhibiting some similarities with reality, but there remains the question of the validity of the forecast in terms of objective methods. One method is to compare the observed data of the validation survey both with the prediction and the initialisation data. The forecast is termed to be successful if the validation fields are closer to the forecast than to the initialisation. In other words, a successful forecast is beating persistence, i.e. assuming that the conditions did not change during the forecast period. In the following, the persistence method is applied by comparing single vertical profiles, horizontal fields

and patterns.

### 5.4.1 *rms* comparison of vertical profiles

The CTD validation survey SOFT-II was conducted in a way that the positions of the casts were identical to the corresponding positions of the SOFT-I initialisation survey (Fig. 2). For forecast skill evaluation, 38 triples were created, each consisting of the validation cast $V$, the corresponding initialisation cast $I$, and a "cast" $F$ extracted from the model forecast at the same position and time when the validation cast was taken. In order to make the casts comparable within each triple, temperature and salinity data were linearly interpolated on 1-m depth levels between the sea surface ($z = 0$; $z$ is the vertical coordinate) and the greatest common depth $z = B$ attained by all three casts. Then, the *rms* difference for temperature between the validation cast $V$ and the initialisation cast $I$ was evaluated as

$$T_{rms}(V,I)_v = \left[\frac{1}{n}\sum_{i=1}^{n}\left[T_V(z_i) - T_I(z_i)\right]^2\right]^{\frac{1}{2}} \tag{1}$$

and the corresponding difference between the validation cast and the cast $F$ from the forecast

$$T_{rms}(V,F)_v = \left[\frac{1}{n}\sum_{i=1}^{n}\left[T_V(z_i) - T_F(z_i)\right]^2\right]^{\frac{1}{2}}, \tag{2}$$

where $n$ means the number of depth levels between $z = B$ and $z = 0$, and the index $v$ indicates that *rms* differences have been evaluated in vertical direction. For salinity the errors $S_{rms}(V,I)_v$ and $S_{rms}(V,F)_v$ were computed accordingly.

For 22 out of the 38 triples, $T_{rms}(V,F)_v < T_{rms}(V,I)_v$ was satisfied, hence at 58% of the CTD positions the forecast was successful. The success is also supported by $\langle T(V,F)_v\rangle = 0.69$°C and $\langle T(V,I)_v\rangle = 0.76$°C, where the expressions in angle brackets represent the mean of $T_{rms}(V,F)_v$ and $T_{rms}(V,I)_v$, respectively, for all 38 casts. For salinity, the situation is similar; also here, the forecast beats persistence in 22 out of 38 cases,

and $\langle S(V,F)_v \rangle < \langle S(V,I)_v \rangle$ is satisfied as well.

### 5.4.2 *rms* comparison of horizontal fields

The previous subsection has indicated that the forecast skill can be a function of depth. To shed more light on this matter, an *rms* comparison of horizontal fields at different vertical levels will be presented.

Such comparison requires that the fields to be compared are mapped on the same horizontal grid and vertical grids. The mapping procedure for the initialisation and validation data sets is OA, applying again a spatial correlation of 20 km, but a temporal correlation scale of 1000 days in order to remove the time dependency. For the initialisation fields, the OA is centred on September 18, 00:00h, and for the validation fields on October 8 00:00h. The *rms* comparison was performed as follows: temperature and salinity of the initialisation and validation casts were mapped on the horizontal model grid at $K = 106$ levels between the sea surface and 500-m depth, starting with a vertical resolution of 1 m in the near-surface layers and then successively increasing to 20 m below 300 m. Because OA does not "know" of horizontal boundaries, values at inactive grid points over land were subsequently masked out in the same way as values below the seabed. For the forecast of October 8, temperature and salinity were linearly interpolated from the model $\sigma$-coordinates onto the same vertical levels. Horizontal *rms* errors of temperature

$$T_{rms}(V,I)_h = \left[\frac{1}{n}\sum_{i=1}^{n}(1-\epsilon_i)[T_V(z_0)_i - T_I(z_0)_i]^2\right]^{\frac{1}{2}} \tag{3}$$

and

$$T_{rms}(V,F)_h = \left[\frac{1}{n}\sum_{i=1}^{n}(1-\epsilon_i)[T_V(z_0)_i - T_F(z_0)_i]^2\right]^{\frac{1}{2}} \tag{4}$$

were evaluated for each level, where $z_0$ is the level depth, $n$ the number of active grid points at that level, and $T_V$, $T_I$, $T_F$ having the same meaning as above. In addition,

basin-integrated values

$$\langle T(V,I)_h \rangle = \left[ \frac{1}{K} \sum_{k=1}^{K} \frac{1}{n} \sum_{i=1}^{n} (1-\epsilon_i) [T_V(z_k)_i - T_I(z_k)_i]^2 \right]^{\frac{1}{2}} \tag{5}$$

and

$$\langle T(V,F)_h \rangle = \left[ \frac{1}{K} \sum_{k=1}^{K} \frac{1}{n} \sum_{i=1}^{n} (1-\epsilon_i) [T_V(z_k)_i - T_F(z_k)_i]^2 \right]^{\frac{1}{2}} \tag{6}$$

were computed. Equivalent computations have been carried out for salinity as well. Note that in (5) and (6), we did *not* just calculate the mean of the *rms* errors at the individual levels according to (3) and (4), because that would bias the result towards the value for the shallower levels containing more grid points. Instead, the integrations were performed first in horizontal and then in vertical direction, assigning each active grid point the same weight. In order to assign a higher weight to those grid points located in the vicinity of the validation casts, the mean square values in the above equations where multiplied by $(1-\epsilon)$, where $\epsilon$ is the normalised OA error for that grid point.

Vertical profiles of the *rms* errors are displayed in Fig. 10. Comparing the black and green curves for temperature in the left panel, the forecast beats persistence in the 20 to 100-m depth range, while below 100 m and right at the surface $T_{rms}(V,F)_h$ is always greater than $T_{rms}(V,I)_h$. For salinity, the situation is different. Here, the forecast beats persistence partly between 80 and 270-m depth. The basin-wide averages for temperature are $\langle T(V,I)_h \rangle$=0.346K, $\langle T(V,F)_h \rangle$=0.333K, and for salinity $\langle S(V,I)_h \rangle$=0.026, $\langle S(V,F)_h \rangle$=0.029. Hence, utilising this method of skill evaluation, the forecast was successful on average for temperature but not for salinity. In order to demonstrate that the data assimilation actually improves the forecast skill, the model run was repeated without assimilation. The corresponding *rms* errors are shown by means of the red curves in 10. Here, it becomes evident both for temperature and salinity that the error of the no-assimilation run is greater than that of the assimilation run; hence, although the salinity

forecast is not successful in terms of the persistence assumption, data assimilation has led to a better forecast.

### 5.4.3 Pattern correlations

The analyses demonstrated above provide a metrics of the distance between two data sets in terms of the *rms* error. However, the error does not contain any information about the structures of the data sets. For example, it could be that the *rms* error between two horizontal temperature fields is extremely small, but the gradient field is quite different. In that case, fronts and eddies would be in different locations among the data sets, i.e. the patterns would be different. Information on the similarity of patterns is provided by correlation analysis in terms of the *pattern correlation coefficient* $P$, which can attain values between -1 and +1. If patterns are similar, $P > 0$, and in case of a perfect correlation, $P = 1$. $P < 0$ means that patterns are not correlated, in the worst case, $P = -1$ (anti-correlation).

Using the same temperature and salinity fields for forecast and initialisation as defined in the previous subsection, we have evaluated the coefficients

$$P_T(V,I) = \frac{\overline{(\mathbf{T}^I - \mathbf{T}^C)^\tau (\mathbf{T}^V - \mathbf{T}^C)}^D}{||\mathbf{T}^I - \mathbf{T}^C||_2 \cdot ||\mathbf{T}^V - \mathbf{T}^C||_2} \tag{7}$$

and

$$P_T(V,F) = \frac{\overline{(\mathbf{T}^F - \mathbf{T}^C)^\tau (\mathbf{T}^V - \mathbf{T}^C)}^D}{||\mathbf{T}^F - \mathbf{T}^C||_2 \cdot ||\mathbf{T}^V - \mathbf{T}^C||_2}, \tag{8}$$

where

$$||\mathbf{T}^I - \mathbf{T}^C||_2 = \left[\overline{(\mathbf{T}^I - \mathbf{T}^C)^\tau (\mathbf{T}^I - \mathbf{T}^C)}^D\right]^{\frac{1}{2}} \tag{9}$$

$$||\mathbf{T}^V - \mathbf{T}^C||_2 = \left[\overline{(\mathbf{T}^V - \mathbf{T}^C)^\tau (\mathbf{T}^V - \mathbf{T}^C)}^D\right]^{\frac{1}{2}} \tag{10}$$

and

$$||\mathbf{T}^F - \mathbf{T}^C||_2 = \left[\overline{(\mathbf{T}^F - \mathbf{T}^C)^\tau (\mathbf{T}^F - \mathbf{T}^C)}^D\right]^{\frac{1}{2}} \tag{11}$$

are the so-called *vector $l_2$ norms* (Strang 2005). $P_T(V,I)$ is the pattern correlation coefficient for temperature, correlating the temperature fields from validation V and initialisation I. The coefficient for the correlation between validation and forecast F is $P_T(V,F)$. Because the correlation coefficients are intended to provide a metrics of the similarity of spatial changes of temperature and salinity, a background field $\mathbf{T}^C$ is subtracted from the matrices $\mathbf{T}^I$, $\mathbf{T}^V$ and $\mathbf{T}^V$ for trend elimination. $\mathbf{T}^C$ is the two-dimensional pattern of temperature "climatology", originating from the OA evaluation of the initial fields, the overbar denotes averaging over the entire domain D, and $\tau$ indicates the transpose matrix.

In case of a successful forecast,

$$P_T(V,I) < P_T(V,F) \tag{12}$$

and

$$P_S(V,I) < P_S(V,F). \tag{13}$$

The resulting vertical structure of pattern correlation coefficients for temperature (Fig. 11, left panel) reveals that the condition for a successful forecast (12) is satisfied almost everywhere in the $\approx$ 20 to 380-m depth range. Only right at the surface and below 380-m depth the persistence assumption does a better job. By contrast, for salinity (right panel) the forecast is successful everywhere between the surface and about 450-m depth. $\langle P_T(V,F)\rangle = 0.347$, the vertical average value of $P_T(V,F)$, is larger than $\langle P_T(V,I)\rangle = -0.098$, indicating that also in terms of the mean pattern correlation the temperature forecast is beating persistence. The corresponding values for salinity are $\langle P_S(V,F)\rangle = 0.575$ and $\langle P_S(V,I)\rangle = -0.192$, hence the forecast of horizontal salinity patterns is even superior to temperature. With respect to the no-assimilation run (red curves), the pattern correlations of the run with assimilation are always higher over most of the 500-m depth range.

# 6 Discussion

The above results have demonstrated the successful setup of an operational forecast system of the Balearic Sea, although the circumstances were not favourable:

- The size of the test area, i.e. the SOFT domain was on the order of only 10% of the water covered model domain (cf. Fig. 1). Therefore, the probability was very high that the structure of the prognostic variables in the interior of the SOFT area were contaminated by false advection from the open boundaries. Assuming a typical advection velocity of 10 cm $s^{-1}$ (cf. Fig. 5) means that the residence time of water particles in the SOFT area was ten days, which is less than the forecast range of 16 days, September 20 to October 6. Hence, within the forecast range the SOFT area was completely flushed by water originating from the surrounding DieCAST model domain. Surprisingly, the forecast beats persistence in five out of six cases, only the *rms* comparison of horizontal fields fails for salinity. Apparently, this positive result is a consequence of the stability of the flow pattern in this region which is mainly oriented parallel to the coast northeast to southwest (Fig. 1). However, one must not interpret the positive results in terms of stable temperature and salinity conditions, because the DieCAST tracer fields were shifted towards the SOFT observations.

- The SOFT-II campaign was cancelled because of bad weather conditions, reducing the number of CTD stations for validation by more than 30% (Fig. 2).

- CTD data covered only the upper about 500-m depth range. This was a critical constraint because no data for assimilation were available below that depth. The consequences can be seen clearly in Fig. 11; both for temperature and salinity the horizontal pattern correlations steadily decrease below about 250-m depth. Due to this shortcoming, the tracer and velocity patterns below 500 m were completely

controlled by DieCAST, apparently impacting also the patterns above. Attempts have been made to get rid of this problem by extending the SOFT initialisation profiles down to the bottom keeping temperature and salinity constant, but that degraded the forecast skill even more.

- The initial conditions were taken from DieCAST, which is based on climatological temperature and salinity distributions, and the open boundaries were as well controlled by DieCAST. The latter appears to be uncritical for the forecast skill in the SOFT area, because the open boundaries of the HOPS domain are far away; nearest to the SOFT area is the open eastern boundary ($\approx$ 100 km), but fortunately it is located downstream of the mean flow (cf. Fig. 5) and therefore odd effects by false advection are unlikely.

- The period of time of 16 days between the end of the initialisation survey (SOFT-I) and the begin of the validation survey and (SOFT-II) was rather long, and one could not anticipate at all an acceptable forecast.

- The forecast range of atmospheric forcing data was limited to 72 hours. This depends on what the utilised atmospheric forecast model is offering. Models other than HIRLAM provide forecast ranges of up to five days or even more, but such long range predictions exhibit only a certain degree of reliability on larger atmospheric scales. In this case of a regional ocean model, any longer range atmospheric forecast probably would not improve the forecast skill. Moreover, it was verified that the impact of atmospheric forcing on the evolution of ocean structures was rather small; the forecast skill of a comparison run without any surface forcing was only insignificantly lower than that of the run presented here, mainly due to slight deviations of temperature and salinity in the near surface layers.

Concerning the atmospheric forcing, there was a discussion among the authors about the general setup of the HOPS run. On the one hand, the setup was favoured which is presented in this manuscript (to be denoted as "Run A") reflecting the situation of scientists or customers having finished the initialisation survey on September 20 and wanting to know immediately the prediction for early October. Therefore, only the atmospheric forecast products through September 23 were applied, representing the realistic situation on that date where no longer range forecasts were available. On the other hand, it was proposed to model the hypothetical situation of a scientist on October 5, who was planning the SOFT-II survey starting next day. In that case, the atmospheric re-analyses through October 5 and the atmospheric predictions through October 8 would have been applied. The advantage of such a setup is obvious - as "good" atmospheric forcing fields would be made available for the period September 21 through October 5, the forecast skill should improve. Therefore, also this setup ("Run B") was tested, but the result is surprising: with respect to the metrics defined above, the basin-integrated skill is even worse in terms of five out of eight statistical parameters (Table 1). The reasons for this result are unknown to the authors but they can be manyfold: bad atmospheric re-analyses fields, bad forecasts for the period October 5–8, non-adequate mixed-layer parameterisation, etc. However, right near the surface the predicted temperature and salinity stratification of Run B were closer to the validation fields than in Run A, indicating that the air-sea heat and water fluxes pushed the model solution into the right direction.

The comparison of Runs A and B has also shown that the model is rather insensitive with respect to the atmospheric forcing. This is supporting the conjecture that the evolution of the interior structure of the ocean is primarily controlled by the internal mass field. Therefore, special care was taken to make the dynamical balance as realistic as possible, utilising the large anticyclone as a test case. More than 30 model runs were made in order

to simulate the movement of the eddy correctly, changing parameters controlling costal and bottom friction and horizontal eddy viscosity and diffusivity. The best of those runs in terms of the skill metrics is Run A presented in this article.

Four different procedures were applied in order to assess the performance of the model, the first three of which are subjective while the fourth one utilises objective methods:

- A comparison of patterns produced by the model with previous knowledge of the Balearic Sea circulation shows good agreement. This is, of course, largely due to the DieCAST model which controls the initial conditions. However after the initialisation, HOPS could have "forgotten" DieCAST rather rapidly and could have developed its own Balearic circulation different from DieCAST. This was not the case – during the 30-day integration period the large scale circulation imposed by the initial conditions did not change significantly except for the SOFT area where the prognostic variables were forced by the assimilation of real data. From another point of view one might interpret this behaviour also as a certain rigidity of HOPS, but this is truly not the case. A comparison of HOPS with other models of the Mediterranean circulation has shown that HOPS is a rather lively model, reproducing more variability than others (N. Pinardi, personal communication).

- In order to assess the capability of HOPS to forecast the evolution of dynamical structures correctly, the predicted sea surface temperature was compared with infrared satellite images. The results were satisfying; the dominant feature of the region, i.e. the large anticyclone, exhibited strong similarities between forecast and observations. This is true both for the passive temperature and for the phase speed of the eddy which is a dynamical quantity.

- For the same purpose, the predicted structures of temperature and salinity were con-

fronted with objectively analysed fields from the validation survey. The agreement was not convincing, but this is no surprise as the tracer patterns in the SOFT-II area are controlled by advection through the open boundaries, flushing the area completely within the forecast period (see above). The same is true for the comparison of the near surface velocity field with directly measured currents. Here, there is an additional mismatch in the south of the SOFT domain, were HOPS predicts a strong coastal current along the Balearic Islands, which could not be detected from the velocity measurements. However, according to Fig. 5, this is apparently not a fault of HOPS: the coastal current is already present in the initial fields on September 10 which were taken from DieCAST.

- The only real hard test to assess the forecast skill of HOPS was performed in terms of three different objective methods. A forecast is denoted as successful if the predicted fields are closer to the (observed) validation fields than the fields used for model initialisation. If the latter were closer to the validation fields, then the persistence assumption (no change) would have been the better forecast. The forecast skill was evaluated for temperature and salinity, and in terms of mean quantities averaged over the SOFT II validation area the forecast was beating persistence in five out of six cases. Concerning the vertical structure of the forecast skill utilising *rms* methods, the forecast is successful at intermediate depth around 100 m, while it is not successful at greater depth and right at the surface. The latter is an indication that either the atmospheric forcing was incorrect or the vertical mixing scheme was inadequate. By contrast, the pattern correlation method was most successful in the upper 400-m depth range, indicating that the predicted structures were right. This provides confidence in the model to reproduce the dynamics correctly.

# 7 Summary and Conclusions

A high-resolution operational forecast system of the Balearic Sea has been developed, based on the Harvard Ocean Prediction System (HOPS). The heart of the system is a primitive equations model formulated in terrain-following $\sigma$-coordinates, complemented by modules managing the assimilation of observational ocean data and an interface to process any type of atmospheric forcing. A special tool was successfully applied which allows the HOPS domain to be one-way nested into any other larger-scale circulation model, and to prevent false advection from open boundaries.

Meridionally, the forecast domain is extending from 38°N to the French coast and in west-east direction from the Spanish mainland to 6°E, comprising the Balearic Sea in the centre, the Gulf of Lions in the north, and the northern part of the Algerian Basin in the south. This setup assures a consistent exchange of water masses of the Balearic Sea with the neighbouring basins. The horizontal resolution of the domain is 2 km, and in the vertical 30 terrain-following layers have been defined in order to resolve the strong shelf slopes along the Balearic Islands and submarine canons at the Spanish mainland coast.

The forecast capability of the system has been validated in terms of a hindcast experiment by means of two oceanographic datasets SOFT-I and SOFT-II, the first of which was collected in mid September and the second in early October 2002. In order to facilitate a smooth startup, the system was initialised from the larger scale DieCAST model and then the SOFT-I data were carefully assimilated. After the nominal time of the end of SOFT-I, the assimilation was continued until the end of September but with steadily decreasing weight. Finally, the system was run in free mode for another ten days and the predicted fields were compared with those structures obtained during SOFT-II. A visual comparison with temperature and salinity fields, directly measured horizontal velocities

and remotely sensed sea surface temperature was satisfactory at best; however, the application of different objective forecast skill evaluation methods impressively demonstrates the forecast capability of the system.

The system is ready to be used as an operational forecast tool of the Balearic Sea. The open boundary and initialisation problem has been solved by one-way nesting of HOPS into the DieCAST model, but the latter can be easily substituted by any other large-scale circulation models, e.g. those being applied in the the MFSTEP project (Pinardi et al. 2003, see also http://www.bo.ingv.it/mfstep/); this requires only to rewrite the interface to map the large-scale model prognostic variables on the HOPS grid. In the same way it is also straightforward to implement any atmospheric forcing other than HIRLAM which was utilised in this study. Three times higher horizontal resolution in special areas of interest may be obtained by two-way nesting, which has been successfully tested (cf. Onken et al. 2003). In order to investigate the spreading of any scalar quantities (pollution, toxic algae, nutrients), HOPS is prepared to forecast the evolution of more passive tracers than just temperature and salinity. Further on, biological modules are available and HOPS can also predict the trajectories of Lagrangian drifters; the latter may be utilised for search and rescue operations and oil spill modelling.

HOPS has been tested on various UNIX platforms, and as far as the authors know, the version described in this paper is the first published one running under LINUX. This improves the portability and operationality of HOPS considerably, because it can be run now on every personal computer even at sea. This version was run on a 3-GHz Pentium IV processor, and the CPU time for the primitive equations model was approximately 50 minutes per model day.

# Acknowledgements

The authors acknowledge the readiness and the skills of the master and the crew of RV Garcìa del Cid, who acquired the observational data sets for the model initialisation and validation. The project SOFT was funded by the European Union under contract number EVK3-CT-2000-00028 within the Framework V programme.

# References

**Álvarez, A., A. Sabates, and J. Tintoré** (1996) Flow modification and shelf-slope exchange induced by a submarine canyon off the northeast Spanish coast. *J. Geophys. Res.*, **101**, C5, 12043–12055.

**Álvarez, A., J. Tintoré, G. Holloway, M. Eby, and J.-M. Beckers** (1994) Topographic forcing of the circulation of LIW in the Western Mediterranean. In: *Seasonal and interannual variability of the Western Mediterranean Sea*, edited by P.E. La Violette, *Coastal and Estuarine Studies Series*, **46**, American Geophysical Union, 361–369.

**Ardhuin, F., J.-M. Pinot, and J. Tintoré** (1999) Numerical study of the circulation in a steep canyon off the Catalan coast (western Mediterranean). *J. Geophys. Res.*, **104**, C5, 11115–11135.

**Brasseur, P., J. Brankart, R. Schoenauen, and J.-M. Beckers** (1996) Seasonal temperature and salinity fields in the Mediterranean Sea: climatological analyses of a historical data set. *Deep-Sea Research*, **43**, 59–192.

**Daniel, P., P. Josse, and P. Dandin** (2005) Further improvement of drift forecast at sea based on operational oceanography systems, in: *Coastal Engineering VII, Modelling, Measurements, Engineering and Mangement of Seas and Coastal Regions*, WIT Press, 13–22.

**Dietrich, D.E., R.L. Haney, V. Fernández, S.A. Josey, and J. Tintoré** (2004) Air-sea fluxes based on observed annual cycle surface climatology and ocean model internal dynamics: a non-damping zero-phase-lag approach applied to the Mediterranean Sea. *J. Mar. Syst*, **52**, 145–165.

**Fernández, V., D.E. Dietrich, R.L. Haney, and J. Tintoré**(2005) Mesoscale, seasonal and interannual variability in the Mediterranean Sea using a numerical model. *Progress in Oceanography*, **66**, 321–340.

**Ferron, B. and J. Marotzke** (2003) Impact of 4D-variational assimilation of WOCE hydrography on the meridional circulation of the Indian Ocean. *Deep-Sea Research Part II: Topical Studies in Oceanography*, **50**, 12–13, 2005-2021, doi:10.1016/S0967–0645(03)00043-2.

**Garciá-Ladona, E., A. Castellón, J. Font and J. Tintoré** (1996) The Balearic current and volume transports in the Balearic Basin, *Oceanol. Acta*, **19**, 5, 489–497.

**Haley, P.J., Jr.** (2001) GRIDS User's Guide, Harvard University, Cambridge, MA, 45pp.

**Haney, R.L.** (1991) On the pressure gradient force over steep topography in sigma coordinate ocean models, *J. Phys. Oceanogr.*, **21**, 610–619.

**Harding, J., C. Martinek, and J. Rigney** (2005) Operational oceanography at the U.S. Naval Oceanographic Office, *Geophys. Res. Abstr.*, **7**, 03689.

**Hoagland, P., D.M. Anderson, Y. Kaoru, and A.W. White** (2003) The economic effects of harmful algal blooms in the United States: estimates, assessment issues, and information needs, *Estuaries*, **25**, 4, 819–837.

**Lermusiaux, P.F.J.** (1997) Error subspace data assimilation methods for ocean field estimation: theory, validation and applications, *Harvard Open Ocean Model Reports*, **55**, Harvard University, Cambridge, MA, 402pp.

**Lozano, C.J., P.J. Haley, Jr., H.G. Arango, Q. Sloan, and A.R. Robinson** (1994) Harvard coastal/deep water primitive equation model, *Harvard Open Ocean Model Reports*, **52**, Harvard University, Cambridge, MA.

**Malakoff, D.** (2004) New tools reveal treasures at ocean hot spots, *Science*, **304**, 1104–1105.

**Millot, C.** (1987) Circulation in the Western Mediterranean Sea, *Oceanol. Acta*, **10**, 2, 143–149.

**Onken, R.**, Robinson, A.R., Lermusiaux, P.F.J., Haley, P.J., Anderson, L.A. (2003) Data-driven simulations of synoptic circulation and transports in the Tunisia-Sardinia-Sicily region. *J. Geophys. Res.*, **108**(C9), 8123, doi: 10.1029/2002C001348.

**Orlanski, I.** (1976) A simple boundary condition for unbounded hyperbolic flows, *J. Comp. Phys.*, **21**, 251–269.

**Pacanowski, R.C., and S.G.H. Philander** (1981) Parameterization of vertical mixing in numerical models of tropical oceans, *J. Phys. Oceanogr.*, **11**, 1443–1451.

**Pinardi N., I. Allen , E. Demirov, P. De Mey, G. Korres, A. Lascaratos, P-Y. Le Traon, C. Maillard, G. Manzella, C. Tziavos** (2003) The Mediterranean Ocean Forecasting System: first phase of implementation (1998-2001). *Annales Geophysicae*, **21**, 3–20.

**Pinot, J.L. López-Jurado, M. Riera, J. Jansá, J. Font, and J. Tintoré** (1998) Time flow variability in the Balearic Channels and its relevance to the western Mediterranean circulation. In: *Rapport Commission Internationale Mer Mediterrannée*, **35**, 188–189, Monaco, CIESM.

**Pinot, J.-M., J. Tintoré, , and D. Gomis** (1994) Quasi-synoptic mesoscale variability of the Balearic Sea, *Deep-Sea Res. I*, **41**, 5/6, 897–914.

**Pinot, J.-M., J. Tintoré, and D. Gomis** (1995) Multivariate analysis of the surface circulation in the Balearic Sea , *Progr. Oceanogr.*, **36**, 343–376.

**Robinson, A.R.** (1996) Physical processes, field estimation and an approach to interdisciplinary ocean modeling, *Earth-Science Rev.*, **40**, 3–54.

**Robinson, A.R.** (1999) Forecasting and simulating coastal ocean processes and variabilities with the Harvard Ocean Prediction System, in *Coastal Ocean Prediction*, edited by C.N.K. Mooers, *Coastal and Estuarine Studies Series*, American Geophysical Union, 77–100.

**Robinson, A.R., H.G. Arango, A. Warn-Varnas, W.G. Leslie, A.J. Miller, P.J. Haley, Jr., and C.J. Lozano** (1996) Real-time regional forcasting, in: *Modern Approaches to Data Assimilation in Ocean Modeling*, edited by P. Malanotte-Rizzoli, *Elsevier Oceanography Series*, **61**, Elsevier, 377–410.

**Robinson, A.R., P.F.J. Lermusiaux, and N.Q. Sloan** (1998) Data assimilation, in *The Sea*, **10**, edited by K.H. Brink and A.R. Robinson, John Wiley & Sons, 541–594.

**Robinson, A.R., and L.J. Walstad** (1987) The Harvard open ocean model: Calibration and application to dynamical process forecasting and data assimilation studies, *J. Appl. Numer. Math.*, **3**, 89–121.

**Shapiro, R.** (1970) Smoothing, filtering, and boundary effects, *Rev. Geophys. Space Phys.*, **8**, 359–387.

**Sloan, N.Q.** (1996) Dynamics of a shelf-slope front: process studies and data-driven simulations in the Middle Atlantic Bight, Ph.D. thesis, Harvard University, Cambridge, MA, 230pp.

**Spall, M.A., and A.R. Robinson** (1990) Regional primitive equation studies of the Gulf Stream meander and ring formation region, *J. Phys. Oceanogr.*, **20**, 985–1016, 1990.

**Strang, G.** (2005) Linear algebra and its applications, 4th ed., Brooks/Cole, 544pp.

# List of Tables

# List of Figures

Table 1: Forecast skill comparison of model runs A (best atmospheric forcing through September 23) and B (best atmospheric forcing through October 8). The better forecast skill for each statistical parameter is printed bold face. The parameters %good T and %good S, respectively, indicate the number of vertical profiles where the forecast beats persistence. For the meaning of the other statistical parameters see text.

| Run | A | B |
|---|---|---|
| %good T | 22 | **25** |
| $\langle T(V,F)_v \rangle$ | **0.69** | 0.72 |
| %good S | **22** | 20 |
| $\langle S(V,F)_v \rangle$ | **0.06** | 0.07 |
| $\langle T(V,F)_h \rangle$ | 0.333 | **0.330** |
| $\langle S(V,F)_v \rangle$ | **0.029** | 0.032 |
| $\langle P_T(V,F) \rangle$ | 0.347 | **0.370** |
| $\langle P_S(V,F) \rangle$ | **0.575** | 0.360 |

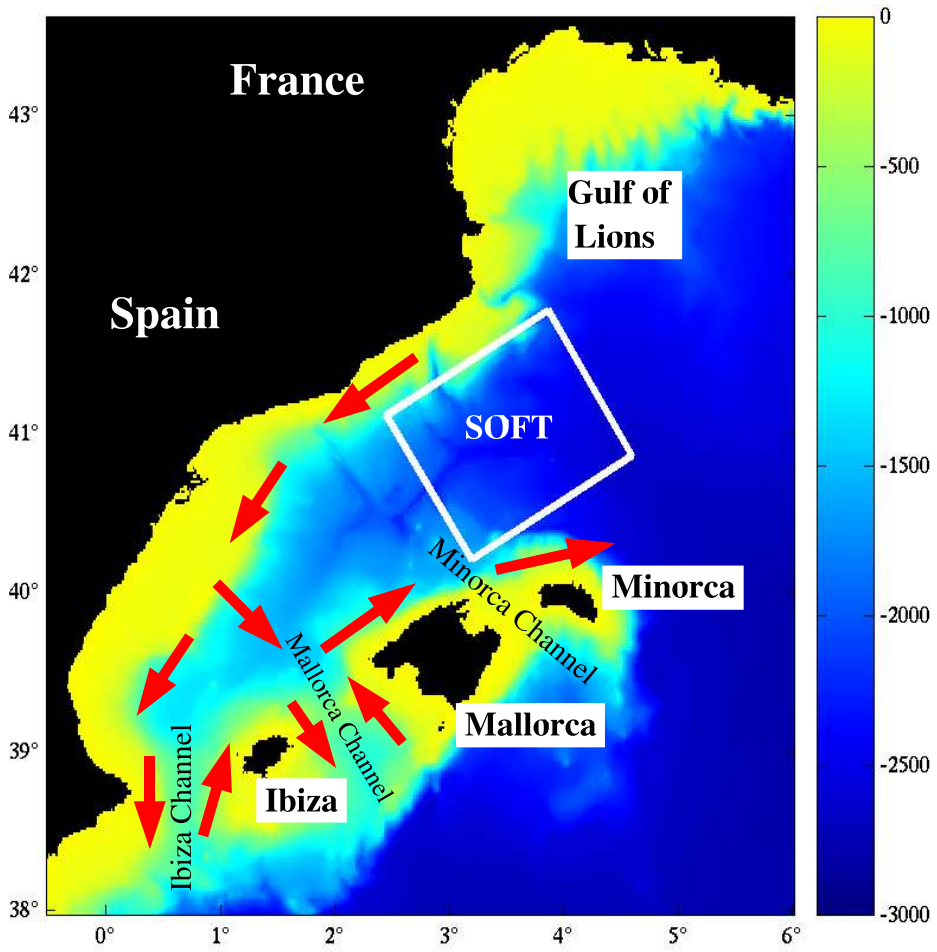


Figure 1: The Balearic Sea. Major surface current regimes are sketched by red arrows, the white rectangle refers to the area of the SOFT campaigns (see text). The area of the chart is identical with the HOPS model domain.

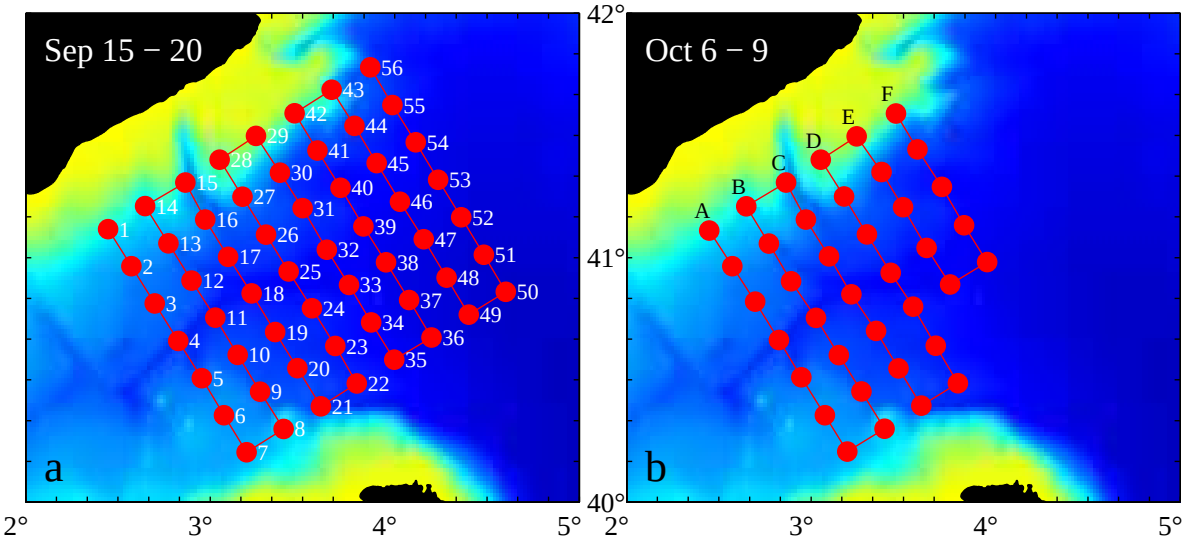


Figure 2: Ship's tracks (red lines) and CTD positions (red dots) of the SOFT-I (a) and SOFT-II (b) surveys. Water depth is indicated by the same colourmap as in Fig. 1. Both surveys started at the most western position. The legs of the SOFT-II survey are denoted by letters A – F.

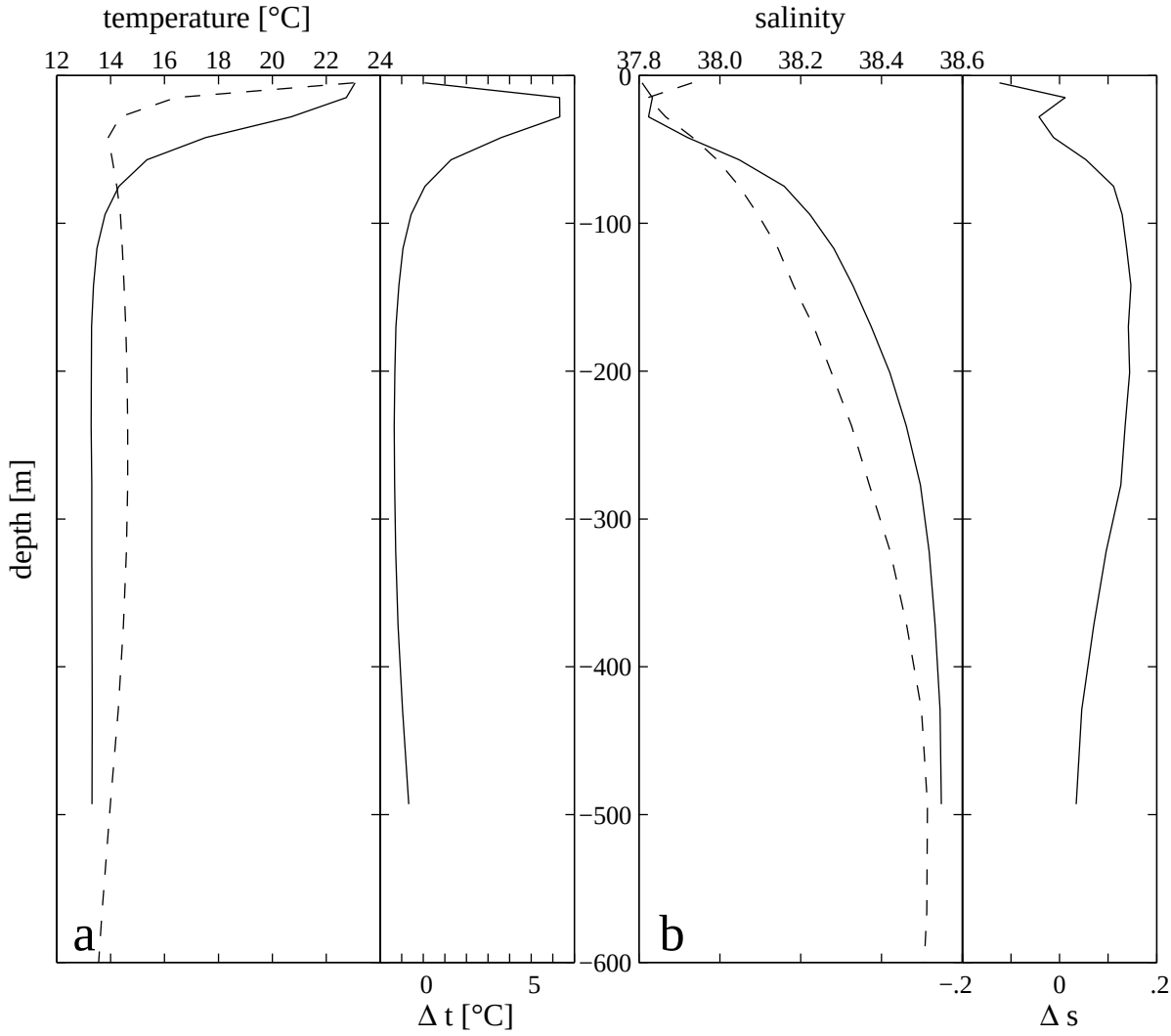


Figure 3: Mean vertical distribution of temperature (a) and salinity (b) during the SOFT-I survey (solid curve) and from the DieCAST model (dashed). The differences of the curves, $\Delta t$ and $\Delta s$, are shown in the right panel of (a) and (b), respectively.

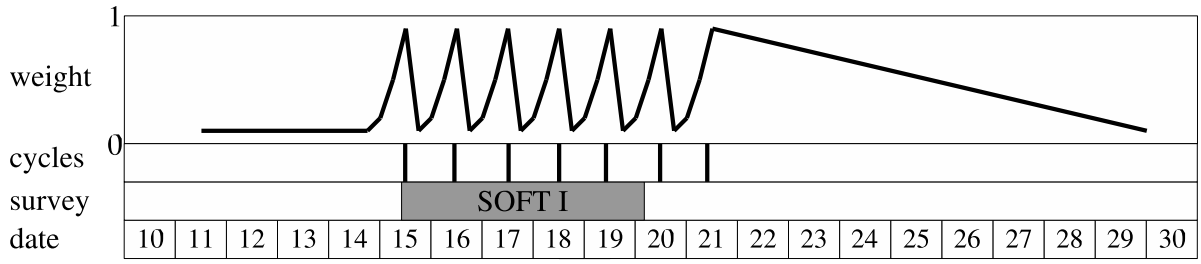


Figure 4: The procedure of assimilating SOFT-I observational data: the September 2002 date is written on the lower panel. The duration of the SOFT-I survey is indicated by the grey bar above. Seven assimilation cycles are created at noon of days 15–21, indicated by the heavy black vertical bars. The top panel graph shows the assimilation weight. Assimilation fields are ramped up towards the following assimilation cycle from days 11 (noon) through 21 (noon) and ramped down after day 21. After the last assimilation on day 30 (00:00h), the model is running without being driven by observations.

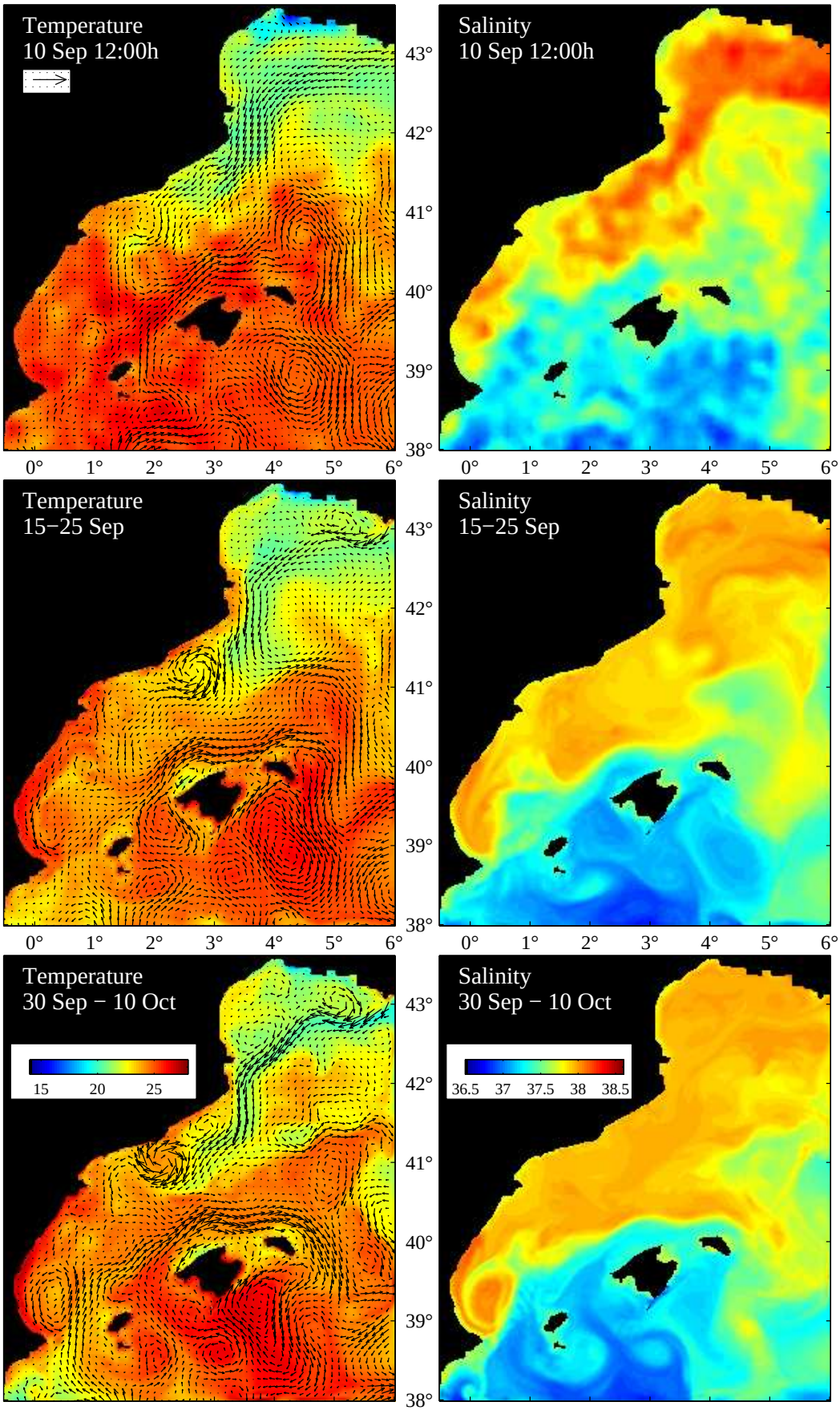


Figure 5: Modelled surface temperature [°C] and total velocity field (left panel) and salinity (right), at initialisation time (top panel), and averaged over the periods of time September 15–25 (centre) and September 30 through October 10 (bottom). Velocity vectors are plotted at 10-km resolution (every 5th vector). The scale vector in the upper left panel represents a velocity of 100 cm $s^{-1}$ .

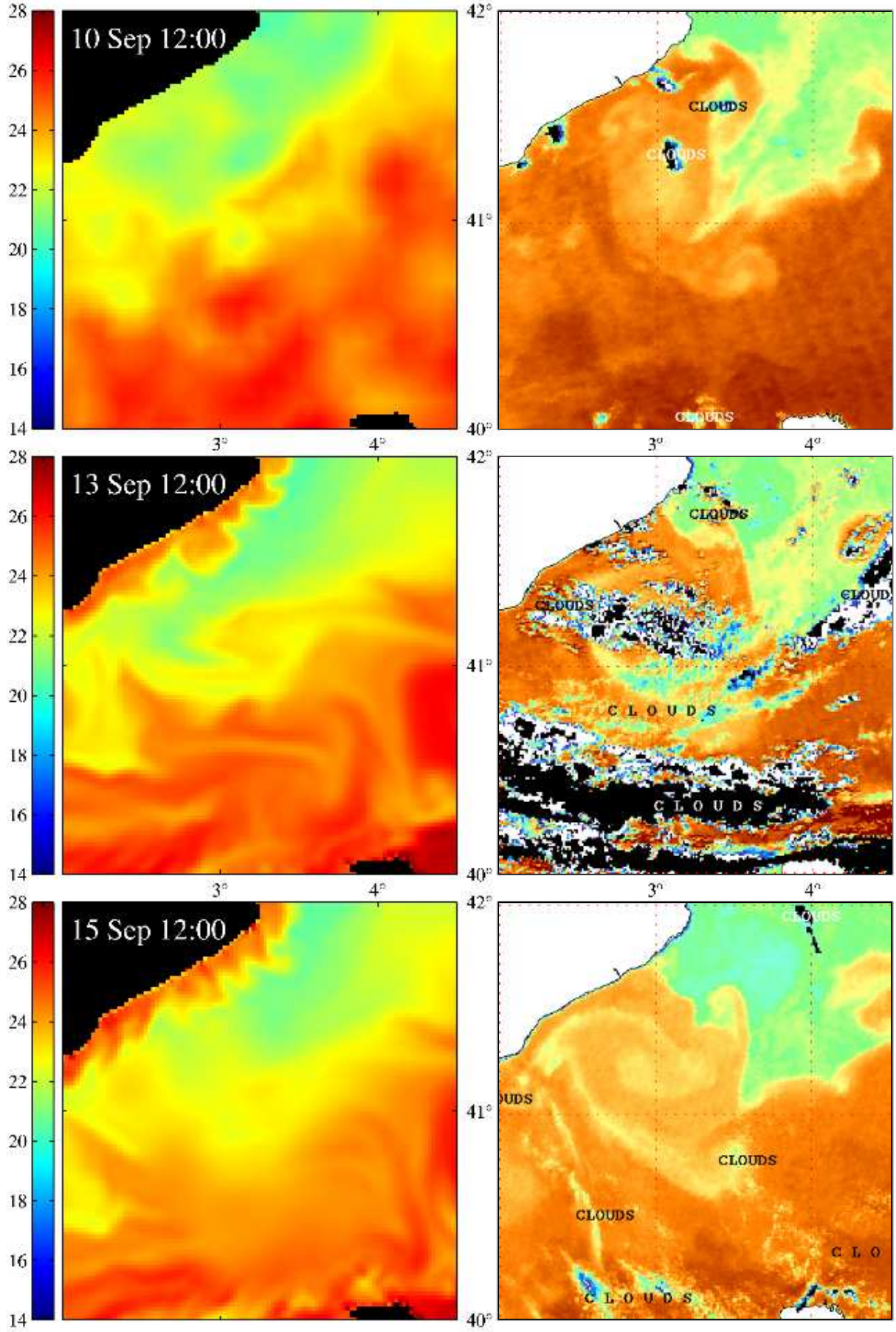


Figure 6: Sea surface temperature [°C] in the SOFT region before the SOFT-I survey took place, simulated by the model (left panel) and observed by satellite (right). The colourmaps in both columns are approximately the same.

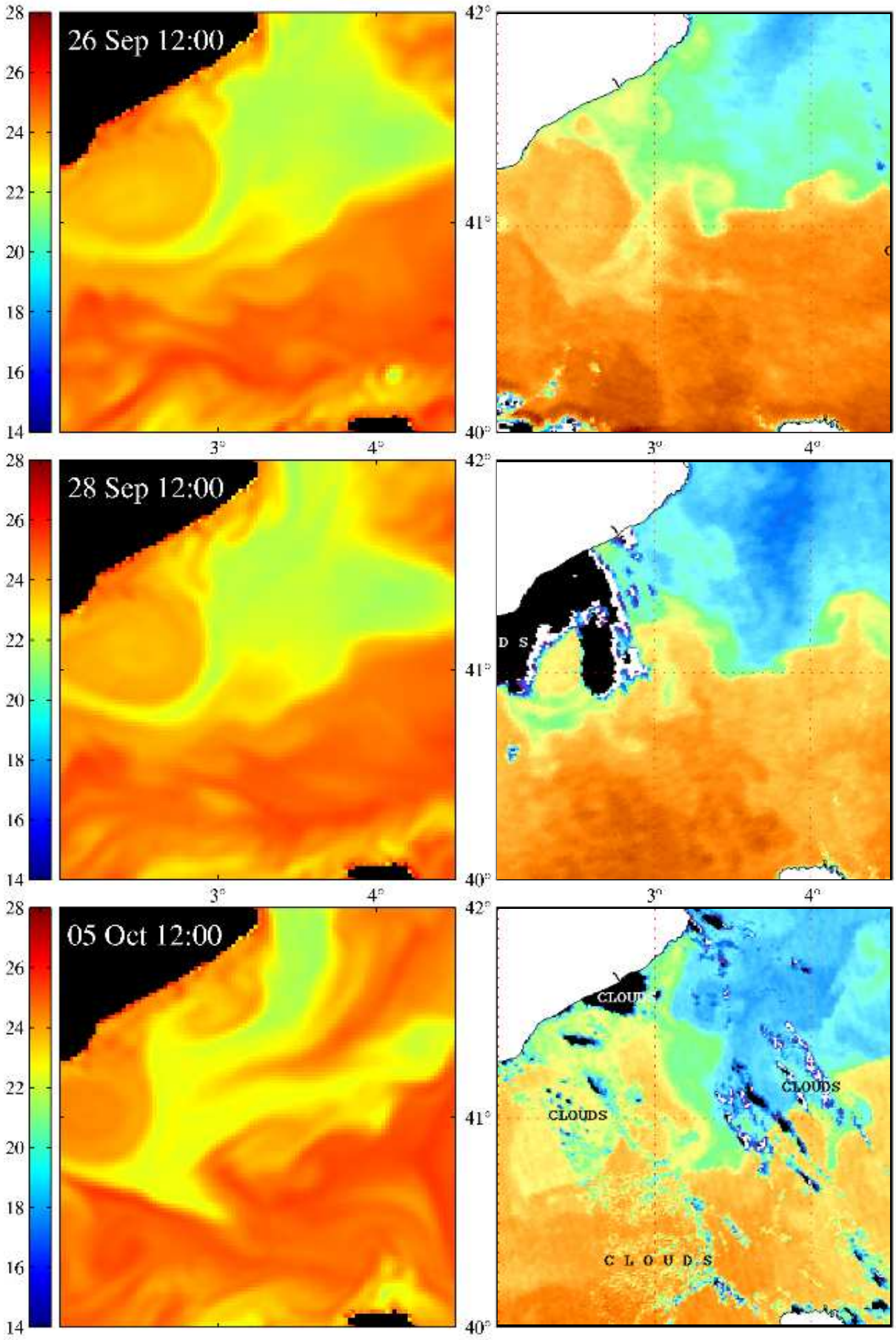


Figure 7: Sea surface temperature [°C] in the SOFT region after the SOFT-I survey took place, predicted by the model (left panel) and observed by satellite (right). The colourmaps in both columns are approximately the same.

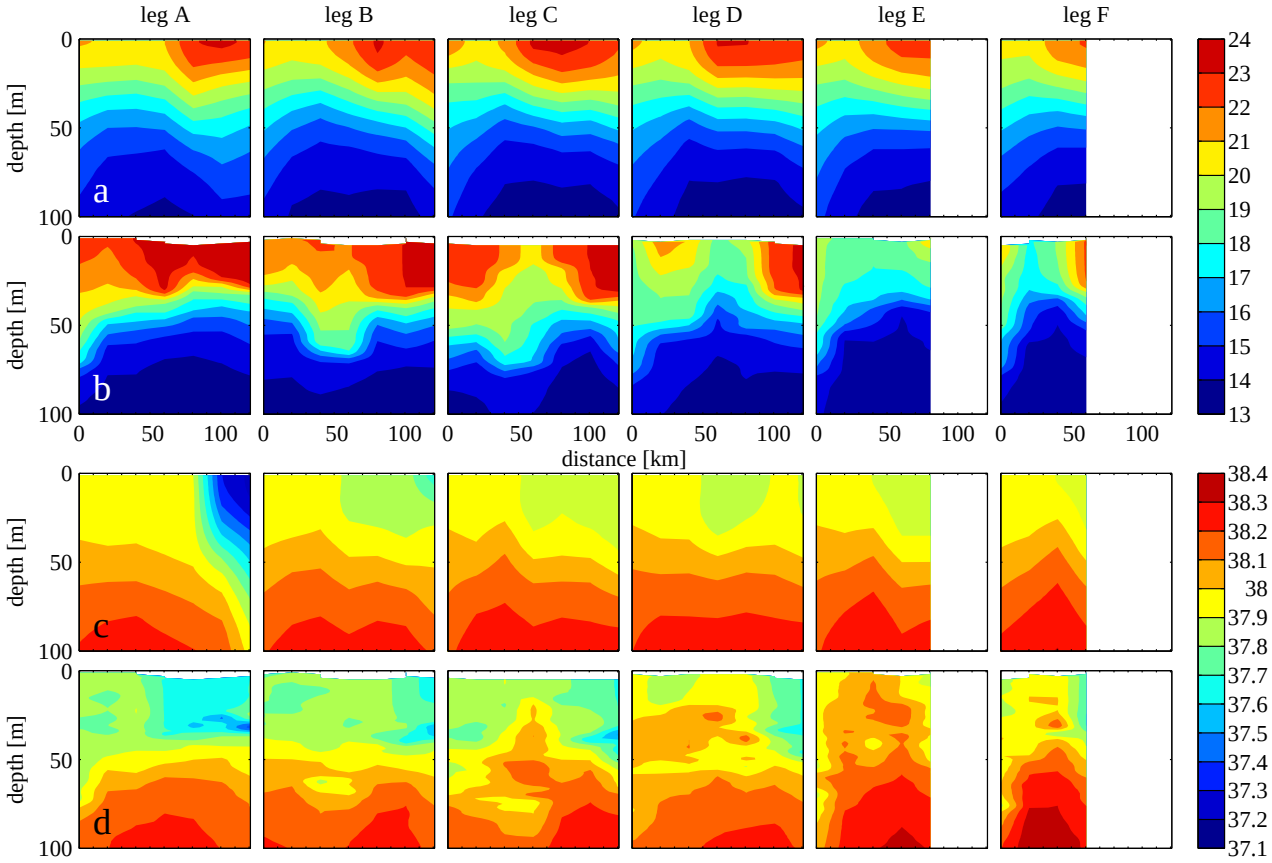


Figure 8: Comparison of predicted and observed temperature [°C] and salinity structures in the SOFT area for the SOFT-II period along survey legs A–F (cf. Fig. 2). The predicted fields (a), (c) were taken from the model as mean fields for the period October 6–9; the corresponding observations are shown in (b) and (d). The horizontal distance refers to the distance from the most northern CTD cast of each leg.

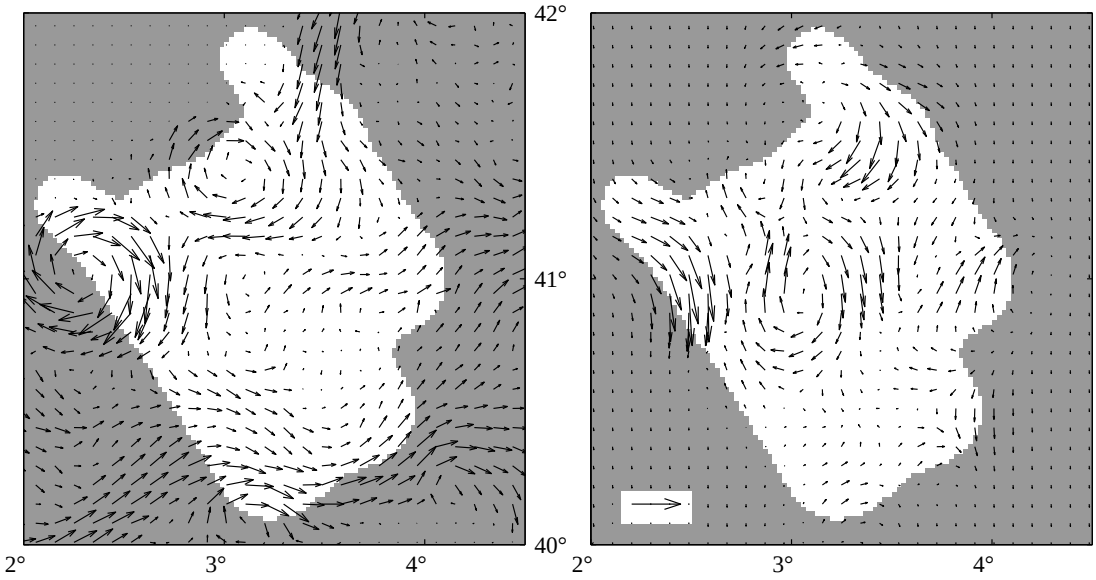


Figure 9: 16 – 25 m vertically averaged and objectively analysed horizontal velocities acquired during the SOFT-II campaign by ship mounted ADCP (right panel) and corresponding velocity fields predicted by the model for noon of October 8 (left). Both ADCP and predicted velocity vectors are scaled identically. The scale vector represents a velocity of 100 cm $s^{-1}$ . Areas where the rms error of the objective analysis exceeds the assumed observational error are gray shaded.

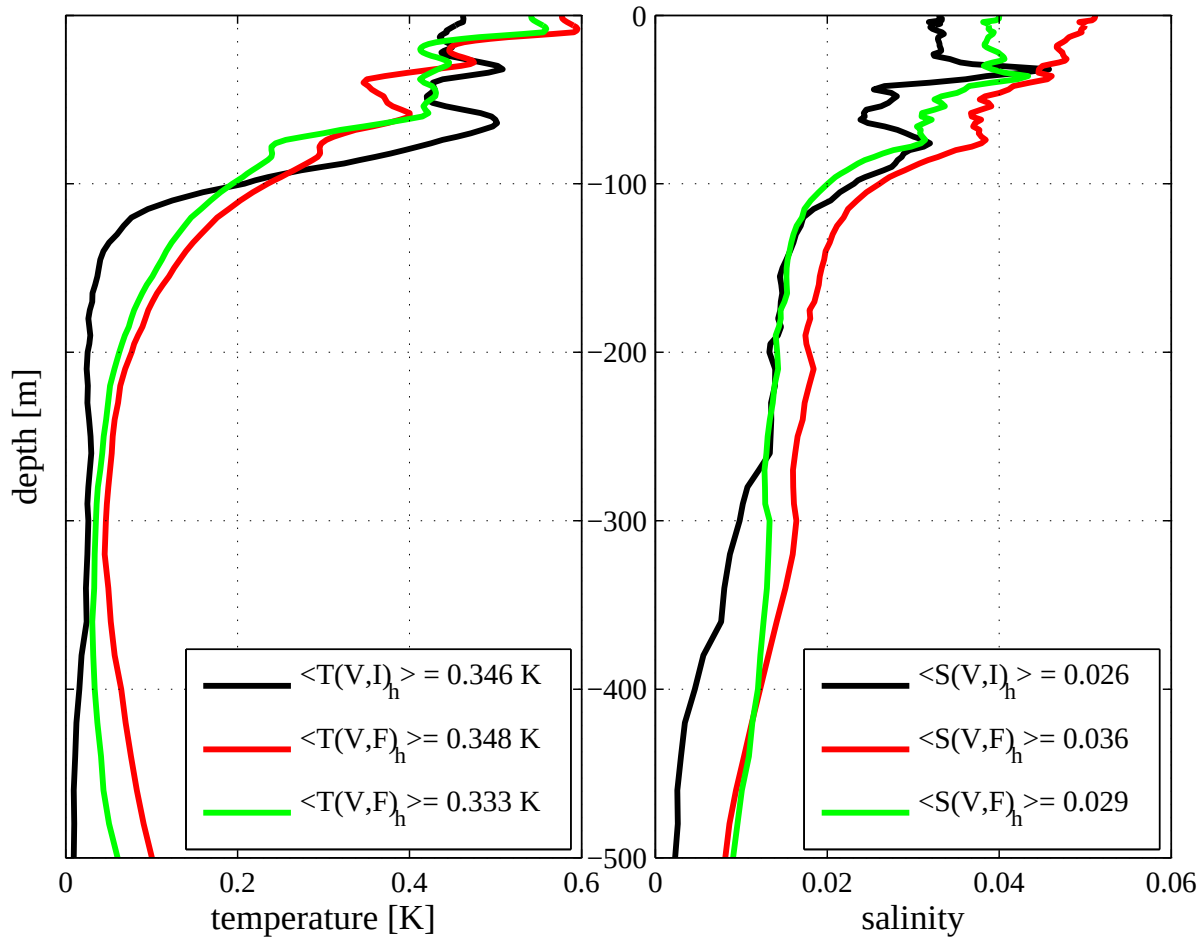


Figure 10: Left panel: vertical structure of $T_{rms}(V,I)_h$ (black line), $T_{rms}(V,F)_h$ for the model run without assimilation (red) and $T_{rms}(V,F)_h$ for the assimilation run (green). The correspondig curves for salinity are in the right panel. The vertically averaged values are written in the legend box of the respective panel.

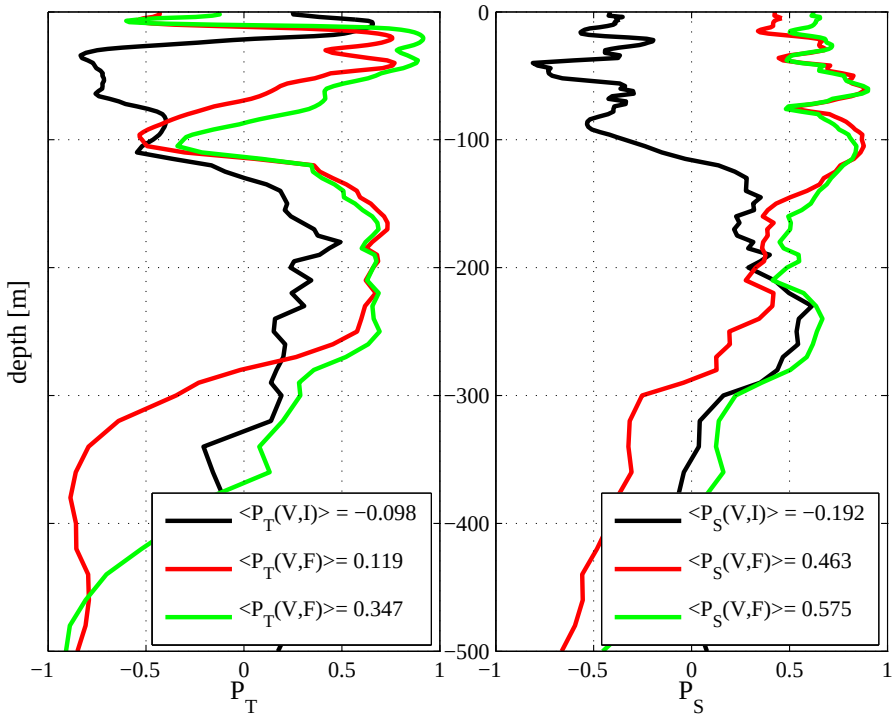


Figure 11: Left panel: vertical structure of $P_T(V, I)$ (black line), $P_T(V, F)$ for the model run without assimilation (red) and $P_T(V, F)$ for the assimilation run (green). The correspondig curves for salinity are in the right panel. The vertically averaged values are written in the legend box of the respective panel.